J|A|C|S
ARTICLES
Published on Web 08/10/2006

Nanografting: Modeling and Simulation

Seol Ryu and George C. Schatz*

Contribution from the Department of Chemistry, Northwestern University, Evanston, Illinois 60208-3113

Received May 4, 2006; E-mail: schatz@chem.northwestern.edu

Abstract: We present a simple phenomenological model of the nanografting process with an emphasis on the formation of binary self-assembled monolayers. This model includes dynamical processes that are involved in natural growth experiments, including molecular deposition, surface diffusion, and the phase transition from physisorption to chemisorption, and we show that it predicts domain formation in ungrafted deposition that matches experiment. The one-order-of-magnitude faster kinetics that is found in the nanografting experiments compared to natural self-assembly (or unconstrained self-assembly) is described with a key assumption that the deposition rate is greatly enhanced in the small region confined between the back side of the AFM tip and the edge of the previously deposited self-assembled monolayer. Monte Carlo simulations based on this model reproduce experimental observations concerning the variation of SAM heterogeneity with AFM tip speed. Our simulations demonstrate that the faster the AFM tip displaces adsorbed molecules in a monolayer, the more heterogeneous are the monolayers formed behind the tip, as this allows space and time for the formation of phase-segregated domains.

I. Introduction

Nanografting technology is a scanning probe lithography method for creating and modifying patterns within self-assembled monolayers (SAMs) on noble metal surfaces.[1,2] The first step, which is called "nanoshaving", involves the displacement of nanometer-scale selected portions of a SAM (which is normally an alkane thiolate on a Au surface) by application of an AFM with a carefully selected force. The desorbed molecules are discarded from the tip-surface contact region, as the solubility of thiols in a solvent such as ethanol or butanol is sufficiently high. The nanoshaving is followed by a second step in which fast self-assembly of alkane thiols from solution onto the newly available open Au surface sites leads to reconstruction of a new monolayer. The use of a different kind of thiol solution in nanografting from the one used to prepare the initial SAM allows one to create nanopatterns within the SAMs.[3−7] Experimental nanografting techniques have advanced significantly in the past few years,[1−10] and as a result, applications of nanografting have been made to nanoelectronic devices, protein patterning, and biosensors. However, many aspects of the nanografting process remain unknown due to the complexity of the fabrication and self-assembly process, and are of interest to fundamental studies.

In normal natural growth experiments (i.e., without grafting), the Au surface is immersed in a thiol solution, and the thiol molecules undergo at least three different steps, called collectively the natural self-assembly (NSA) mechanism,[8,11] to produce nearly complete SAM structures. Thiol molecules diffusing in the solution phase first arrive at the Au surface in lying-down configurations. This is followed by surface diffusion as the second step, and then the molecular configuration transforms from lying-down to standing-up as Au−S chemisorption occurs. For the case of nanografting, however, Liu and co-workers have suggested that the adsorbing thiol molecules undergo a modified deposition process in the region behind the AFM tip.[9] In their in situ nanografting experiments,[9] they found that the SAM patterns obtained using nanografting are nearly free of surface defects such as scars and pinholes, and in addition, the kinetics of deposition/chemisorption is much faster than in the natural-growth process. They proposed that this "accelerated kinetics" originates from a different reaction pathway, called the spatially confined self-assembly (SCSA) mechanism. In this case, molecular translational or rotational degrees of freedom are restricted in the spatially confined microenvironment between the moving AFM tip and the SAM edges. This confinement leads to preferential adsorption in the standing-up configuration. Ascertaining the validity of this SCSA mechanism requires an understanding of many issues concerning the shaving/deposition/diffusion/chemisorption process, including the answer to questions such as how fast do the molecules move into the confined environment and how fast

(1) Liu, G.-Y.; Xu, S.; Qian, Y. *Acc. Chem. Res.* **2000**, *33*, 457.
(2) Xu, S.; Liu, G.-Y. *Langmuir* **1997**, *13*, 127.
(3) Cruchon-Dupeyrat, S.; Porthun S.; Liu, G.-Y. *Appl. Surf. Sci.* **2001**, *175*, 636.
(4) Liu, M.; Amro, N. A.; Chow, C. S.; Liu, G.-Y. *Nano Lett.* **2002**, *2*, 863.
(5) Liu, J.-F.; Cruchon-Dupeyrat, S.; Garno, J. C.; Fommer, J.; Liu, G.-Y. *Nano Lett.* **2002**, *2*, 937.
(6) Brower, T. L.; Garno, J. C.; Ulman, A.; G.-Y. Liu; Yan, C.; Gölzhäuser, A.; Grunze, M. *Langmuir* **2002**, *18*, 6207.
(7) Wadu-Mesthrige, K.; Xu, S.; Amro, N. A.; Liu, G.-Y. *Langmuir* **1999**, *15*, 8580.
(8) Xu, S.; Cruchon-Dupeyrat, S. J. N.; Garno, J. C.; Liu, G.-Y.; Jennings, G. K.; Yong, T.-H.; Laibinis, P. E. *J. Chem. Phys.* **1998**, *108*, 5002.
(9) Xu, S.; Laibinis, P. E.; Liu, G.-Y. *J. Am. Chem. Soc.* **1998**, *120*, 9356.
(10) Yu, J.-J.; Tan, Y. H.; Li, X.; Kuo, P. K.; Liu, G.-Y. *J. Am. Chem. Soc.* **2006**, *128*, 11574.
(11) Poirier, G. E.; Plyant, E. D. *Science* **1996**, *272*, 1145.

do they chemisorb compared to the lying-down thiol molecules in the natural-growth experiments.

On the theoretical side, it is interesting to note that, while some theory and simulation work[12−15] on both pure and mixed binary SAM structures has been reported, nanografting has never been studied. The purpose of this work, therefore, is to develop a theoretical model for nanografting and, through dynamical simulations based on this model, to provide a framework for understanding the various rate processes involved. This will be accomplished using a coarse-grained kinetics model which provides sufficient level of detail that the atomic level mechanisms important in nanografting can be identified.

Of course, one of the typical problems with modeling systems with self-assembled monolayers and nanografting is that complex molecules such as alkane thiols are too big for any practical atomistic dynamics simulation.[15] Also, the time scale with which the deposition and diffusion of thiol molecules takes place is sufficiently large that meaningful molecular dynamics calculations are not feasible. To circumvent these problems, we will use a phenomenological coarse-grained model in which the Au surface is treated as a two-dimensional square lattice and thiol molecules are simple dots that undergo random-walking between lattice sites. Various dynamical processes can occur at the surface, such as particle deposition, surface diffusion, and the molecular phase transition from lying-down to standing-up configurations. These processes as well as the speed and size of the nanografting tip will be introduced with a minimal set of parameters, i.e., creating, deleting, and immobilizing dots at lattice sites. One of the advantages of this model is that the entire growth of the SAMs is broken down into various individual dynamical processes we can control, which makes it easy to identify the direct consequence of each process in creating the SAM patterns.

From the viewpoint of mechanistic analysis, binary mixed SAMs are more useful than pure ones because the degree of mixing of the two kinds of thiols in the final SAM patterns directly reflects the relative importance of the different dynamical processes involved in SAM formation. Recent experimental studies by Liu and co-workers[10] have provided us with better insight into the mechanisms of nanografting. After they prepared various binary mixed SAMs having large domain structures using solutions of long- and short-chain thiol molecules by the natural growth method, they performed a series of nanografting experiments with varying AFM tip speeds in the mixed thiol solution. The calculations demonstrated that the lateral heterogeneity of the nanografted area can be controlled at the nanoscale by controlling the tip speed. This makes the nanografting procedure potentially a useful technique for effective manipulation of biomembrane structures.

Our model starts with the binary mixed SAMs of ref 10 (here denoted the "companion paper") for the model system to which our modeling and simulation of nanografting procedure is parametrized. A focus of our studies will be on two of the most interesting features of nanografting experiments with mixed SAMs, namely nanometer-scale local control over the lateral heterogeneity or domain sizes and, parallel to the work of ref 10, the accelerated kinetics that was mentioned earlier.[9,10] We will discuss what kinds of assumptions and interpretations are needed in order to reproduce these two features simultaneously in the simulation.

In the following section, we will briefly mention the portion of the companion paper we want to simulate and then explain in detail how the individual dynamical processes are modeled with reasonable values for the parameters. Next, we will show and discuss the simulation results in the context of the experimental work. We summarize our work in the final section.

II. Modeling of Dynamics

In the companion paper,[10] Liu and co-workers applied the nanografting technology to a Au surface in which binary mixed thiol solutions are used to regulate binary SAM surface structures at the nanometer scale, after first preparing a natural-growth, binary mixed SAM. Thus, in the first step, a mixed C_{18}/C_{10} solution (C_n represents a normal alkane thiol with n being the number of carbons in the chain), with $[C_{18}] + [C_{10}] = 2\ \mu$M and $[C_{18}]:[C_{10}] = 3:5$, is used in a NSA process (i.e., immersing the Au substrate in the mixed thiol solution) to make monolayers of approximately 3:1 mixed surface composition having C_{18} domain structures that have a diameter of about 8 nm. Then they demonstrated that nanografting using different fabrication tip speeds in the range of $0.02-10\ \mu$m/s can regulate the heterogeneity of the binary mixed SAMs. While a nanografted SAM produced at a fast tip speed of 10 μm/s was close to the one prepared from natural growth, a nearly molecular-level mixing of the two kinds of thiols was achieved with a very slow speed of 0.5 μm/s or less. It is believed that this observation is highly correlated with a kinetics change from SCSA to NSA as the tip speed increases.

In our modeling and simulation, we will try to understand the relationship between the two distinctive features of binary system nanografting, "nanoscale local control" of heterogeneous SAM structures and "fast kinetics", that make the nanografting technique a quick and useful fabrication tool for creating and modifying SAM structures.[1,10]

The actual Au(111) surface is a two-dimensional hexagonal lattice of thiol adsorption sites with lattice spacing $l = 5$ Å. Since details of the lattice structure are unlikely to be important, we chose to use a two-dimensional square lattice of size 101×101 (50×50 nm^2, with $l = 5$ Å) with periodic boundary conditions for our calculations. The 101×101 lattice is the size of lattice we can routinely use for simulating SAM formation, given that, with a constant deposition probability P at each empty site for each simulation time step, the total number of time steps needed to form a complete monolayer is given approximately by log(the number of lattice sites) divided by P.

In the following subsections, we will describe how the individual fundamental dynamical processes are modeled with a minimal set of parameters. In addition, we will assign standard values to those parameters, taking into account the usual experimental conditions. For reference, Table 1 summarizes all the parameters used in the simulation.

II.a. Deposition. We define the physisorption state of a dot or particle at each lattice site as a state in which the particle can execute random-walking, whereas chemisorption represents immobilization of the particle. We assume that all particles are

(12) Shevade, A. V.; Zhou, J.; Zin, M. T.; Jiang, S. Y. *Langmuir* **2001**, *17*, 7566.
(13) Aoki, K. J. *Electroanal. Chem.* **2001**, *513*, 1.
(14) Mizutani, W.; Ishida, T.; Tokumoto, H. *Appl. Surf. Sci.* **1998**, *132*, 792.
(15) Hautman, J.; Klein, M. L. *J. Chem. Phys.* **1989**, *91*, 4994. Siepmann, J. I.; McDonald I. R. *Mol. Phys.* **1992**, *75*, 255.

Table 1. Summary of the Parameters for the Individual Dynamical Processes and Their Standard Values

	Lattice
$L = 50$	lattice sites $\in\{(x,y)\mid -L \le x \le L, -L \le y \le L\}$ unit lattice spacing representing $l = 5$ Å
	Surface Diffusion
$\Delta t = 10^{-6}$ s	diffusion time scale = unit time in simulation
$\epsilon/k_BT = 1$	stickiness between thiols of same kind
	Deposition
$k_{C18} = k_{C10} = 5\ s^{-1}$	deposition rate constants, and so $P = (k_{C18} + k_{C10})\Delta t$ = deposition probability during Δt
	Phase Transition
$A_m = 10^{11}\ s^{-1}$	amplitude of frequency factor
$\theta_{loc}^{c} = 0.9$	critical local coverage
$f = 20$	sharpness of transition
$l_{C10} = 4l$	effective chain length of C_{10}
$l_{C18} = 6l$	effective chain length of C_{18}
$E_c = 30$ kJ/mol	activation energy for transition
	Nanografting
$r_{tip} = 10l$	flat tip width = $2r_{tip}+1$
$v = 10^{-3}\ l/\Delta t$	tip speed
$P_s = 0.01$	enhanced deposition in confined environments immediately behind the AFM tip
$\xi = 5l$	size of confined environments to be effective for enhanced deposition

initially in their physisorption state upon deposition, and eventually undergo phase transition from physisorption to chemisorption. (See below for the conditions needed for this molecular phase transition.) The desorption process will be ignored because the activation energy for desorption is about twice as large as the one (~30 kJ/mol) for adsorption.[8,16] We assume a constant deposition probability $P = k\Delta t$ at bare surface sites, where k (s^{-1}) is the experimental adsorption rate of thiol molecules from the solution phase, and Δt (s) is the unit time for simulation. Δt is considered to be the time scale for the fastest dynamical process in the simulation scheme, and thus it will be the (unknown) surface diffusion time scale for physisorbed species in our case. A reasonable guess for Δt will be 10^{-9} to 10^{-6} s, as explained below. Note that the constant deposition assumption alone results in a Langmuir-type exponential increase in coverage with time, i.e. $\theta = 1 - \exp(-kt)$.[16] For particle deposition on the lattice, every empty site at every moment in simulation will be filled with a probability P.

For a binary solution of the thiols A and B, the assumption $k_A = k_B$ naturally leads to a 1:1 binary mixed SAM in the kinetic regime. The numerical values of k_A and k_B can be made equal to each other by adjusting the relative concentrations of the two thiols, C_A and C_B, in solution, using the relationships $k \cong k_{intrinsic}C$ and $k_{intrinsic} = S_0 v_T$ where C is the thiol solution concentration, S_0 is the sticking coefficient for the thiol molecule, and $v_T = \sqrt{k_BT/2\pi m}$ is the mean thermal velocity toward surface with m being the mass of the thiol.[16] Normally, longer chains have higher sticking probabilities S_0 toward the Au surface. This can be described by the empirical law $S_0 = P_0 \exp(bN_{CH_2})$, where, in ethanol solution, $P_0 = 1.26 \times 10^{-8}$, $b = 0.26$ per methylene group, and N_{CH_2} is the number of methylene groups excluding the terminal methyl group.[16] Thus, when we want to make a 1:1 mixed SAM from a short/long binary thiol solution, the short-chain thiol concentration should be higher than the long-chain thiol concentration.

(16) Jung, L. S.; Campbell, C. T. *J. Phys. Chem. B* **2000**, *104*, 11168.

In the companion paper,[10] Liu and co-workers used 3:5 C_{18}/C_{10} alkane thiol solutions to force $k_{C18} \approx 3k_{C10}$. Specifically, in the case where $[C_{18}] + [C_{10}] = 2\ \mu$M with $[C_{18}]$:$[C_{10}] = 3:5$, they have $k_{C18} = 0.0038\ s^{-1}$ and $k_{C10} = 0.0010\ s^{-1}$,[10,16] leading to a mixed monolayer composition C_{18}:C_{10} = 38:10.

These deposition rates are, however, too slow to form monolayers on a practical time scale for our simulations so we have chosen $k_A = k_B = 5\ s^{-1}$, so that $P = (k_A + k_B)\Delta t = 10^{-5}$ for the largest value of Δt that we think applies to the problem of interest, $\Delta t = 10^{-6}$ s. (This Δt value will be explained in the next section.) Thus, our assumed rates are over 1000 times higher in absolute value than in the experiments. However, only the relative values of these rates (relative to the diffusion time scale) are important in our model.

II.b. Surface Diffusion. We assume that the particles execute a random-walk every time step, Δt, but subject to nearest-neighbor interactions. The latter leads to a probability for moving to an open destination given by $\exp(-n_s\epsilon/k_BT)$, where n_s is the number of particles immediately adjacent to the original site and ϵ is an interaction energy. Here we assume that there are stabilizing interactions between particles when they are right next to each other that inhibit diffusion. ϵ/k_BT is a parameter of the model, and we assume, typically, that this has the value 1. This means that the probability of diffusion is 1 if there are no adjacent particles, $1/e$ for one, $1/e^2$ for two, and $1/e^3$ for three adjacent particles.

In the binary thiol system, one may expect to have three different ϵ values, ϵ_{AA}, ϵ_{BB}, and ϵ_{AB}, whose relative strengths determine the domain sizes. A realistic but asymmetric interaction model [where $\epsilon_{AA} = \epsilon$ and $\epsilon_{BB} = \epsilon_{AB} = 2\epsilon/3$ (A = C_{18} and B = C_{10}) may be made, assuming that the interactions between longer chains are enthalpically stronger than the others in proportion to the chain length ratio] is $l_{c10}/l_{c18} \approx 2/3$. This model will lead to C_{18} domain formation in the mixed binary SAMs, as observed in experiments,[10] because the driving force for domain formation is the ~1.5 times stronger interaction between C_{18} chain neighbors.[17]

An alternative intermolecular interaction model is the symmetric scheme, $\epsilon = \epsilon_{AA} = \epsilon_{BB}$ and $\epsilon_{AB} = 0$, where it is assumed that same species molecules tend to stick together due to a combination of enthalpic and entropic effects. We find that this model leads to clearer particle segregation, and thus the domain structures in the binary SAMs are much easier to identify than in the asymmetric model.

The choice between the two interaction models does not affect the overall conclusions of this work as both models lead to domain formation and both models require additional assumptions to give the enhanced deposition that arises in nanografting.

In our simulation, we use the symmetric interaction model, as this makes it easier to quantify domain sizes and their changes. The parameter ϵ/k_BT controls domain formation so that higher values tend to suppress surface diffusion, leading to smaller domains, while smaller values lead to larger domains. Our choice for $\epsilon/k_BT = 1$ is for convenience, given the number of lattice sites that we have chosen to study, but as we shall see it, leads to realistic domain size results.

(17) The asymmetric interaction model where $\epsilon_{AA} = \epsilon = k_BT$ and $\epsilon_{BB} = \epsilon_{AB} = 2\epsilon/3$ leads to more diffuse domain structures due to the smaller driving force for particle segregation, but the average domain radius is found to be close to that of the symmetric model. Simulation results for the asymmetric model can be found in Supporting Information.

The correct value of the surface diffusion time scale Δt for alkane thiols is basically unknown, but it can be approximately calculated using the two-dimensional Einstein−Smoluchowski eq $4D\Delta t = l^2$, once we estimate the surface diffusion constant D and taking $l = 5$ Å to be the lattice spacing. Using $D = 8.4 \times 10^{-15}$ m^2/s from ref 18 (assuming that the thiol molecules at the moving boundary of dip-pen nanolithography patterns are still in the physisorbed state), we get $\Delta t = 7.4 \times 10^{-6}$ s. Another estimate of $D = 7 \times 10^{-12}$ m^2/s from thiol diffusing on poly(dimethylsiloxane) in ref 19 gives $\Delta t = 8.9 \times 10^{-9}$ s. The latter estimate was used for a thiol diffusing on a thiol monolayer in the dip-pen modeling in ref 20. These estimates suggest that $\Delta t = 10^{-6}$ s or shorter. To make the simulation feasible, we have taken $\Delta t = 10^{-6}$ s as the standard value.

II.c. Two-Dimensional Phase Transition. Physically, the two states of a particle, physisorption and chemisorption, can be associated with two different molecular configurations on the surface. Most likely, the physisorption state is when the thiol molecule is lying down, and the chemisorption state is when the thiol molecule is standing up, forming a Au−S bond to become part of the SAM. The rate at which the physisorbed thiols undergo phase transition to become chemisorbed depends on the conditions of the experiment. We believe that the transition rate for a particular physisorbed thiol molecule depends on the local lateral pressure that the molecule feels. Since the local pressure that the molecule feels is directly proportional to the local coverage θ_{loc} in the neighborhood of the molecule, we assume that, when the local coverage θ_{loc} equals a certain critical value θ_{loc}^c, the molecule transitions to its chemisorption state, and the random walking stops.

The transition rate for chemisorption can be written in the Arrhenius form $k_c = A(\theta_{loc}) \exp(-E_c/RT)$ where E_c is the activation energy for the transition and $A(\theta_{loc})$ is the frequency factor. E_c is experimentally known to be about 30 kJ/mol nearly independent of thiol chain lengths,[21] but $A(\theta_{loc})$ is unknown; therefore, we model $A(\theta_{loc})$ in the following fashion. We assume that $A(\theta_{loc})$ depends on θ_{loc} in a similar way to the dependence of the lateral pressure of a Langmuir−Blodgett (LB) film on coverage.[22] Thus, we use the functional form $A(\theta_{loc}) = 0.5A_m \cdot \{1 + \tanh[f \cdot (\theta_{loc} - \theta_{loc}^c)]\}$, as shown in Figure 1A, to mimic the lateral pressure transition. The local coverage θ_{loc} for a molecule is defined as the coverage in a neighborhood that is taken to be a circular area with the molecule at the center and with radius equal to its effective molecular length, l_{c10} or l_{c18}. The critical local coverage θ_{loc}^c is a simulation parameter that determines when the physisorption-to-chemisorption transition takes place, and the sharpness factor f is another parameter that controls the range of the transition. The frequency factor amplitude A_m is another unknown, but we can estimate its order-of-magnitude value using typical values for the lateral pressure of saturated Langmuir−Blodgett (LB) films composed of long-chain lipids, 10−50 mN/m,[22] and the harmonic approximation. If one assumes that the mass of the thiol molecules (C_{10} or C_{18}), 10^{-25} kg, is confined to a harmonic well with this force constant, we have $A_m = A(\theta_{loc} = 1) \approx (2\pi)^{-1} \sqrt{k/m} = 10^{10}-10^{11}$ s^{-1}.

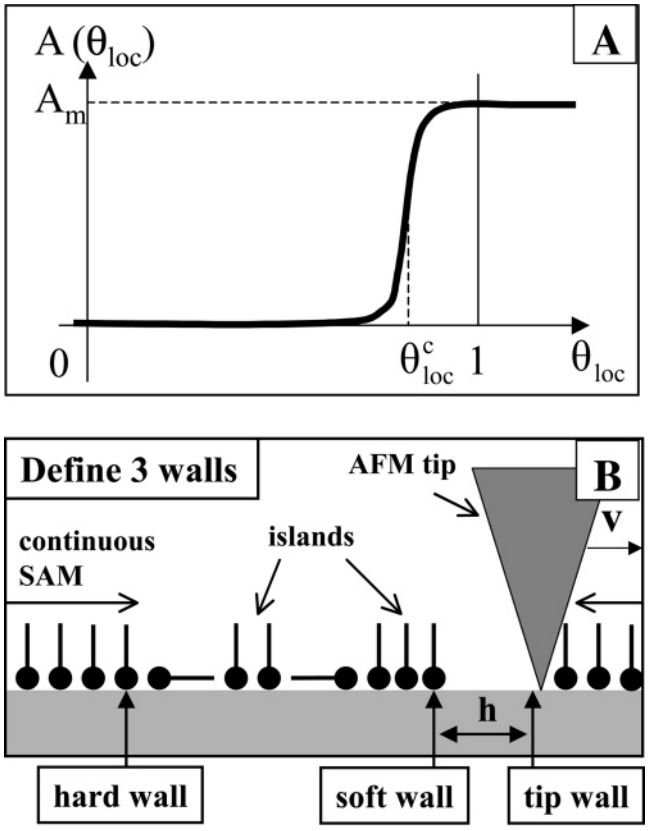

Figure 1. [A] Functional form of the frequency factor $A(\theta_{loc})$. [B] Schematic snapshot of the nanografting process.

A direct consequence of this model is that chemisorption eventually dominates, leading to a complete monolayer containing only chemisorbed molecules. The one exception to this is when there is only one molecule on the surface. This phenomenological phase-transition model is put into play in our simulations, as this allows physisorbed molecules to perform surface diffusion until near monolayer coverage, and then to undergo phase transition into the chemisorbed state, which is similar to what is observed experimentally.[8]

In the simulations, we set $A_m = 10^{11}$, $\theta_{loc}^c = 0.9$, and $f = 20$ and consider the lengths of the C_{10} and C_{18} thiols as $4l$(17.3 Å) and $6l$(27.7 Å), respectively. Typical θ_{loc}^c values are 0.8 or higher,[8] and we can set $f = 20$, so that we have a 96% chance to find $A(\theta_{loc})$ in the range of $\theta_{loc} \in [\theta_{loc}^c - 0.1, \theta_{loc}^c + 0.1]$. The inverse of the rate constant may be called the variable lifetime $\tau_c = 1/k_c$. In our simulations, we apply the rule that, for every diffusion time step, Δt, the probability of a particle being chemisorbed is $1 - \exp(-\Delta t/\tau_c)$, with the lifetime τ_c depending on local coverage.

II.d. Nanografting: Tip Shape and Speed. After a complete monolayer forms, we assume that a chisel-like flat tip of a certain width $(2r_{tip} + 1)$ scrapes away the adsorbed molecules as it moves along the surface. The shaving-tip speed in the experiments is typically $v = 1$ μm/s. With a lattice spacing $l =$ 5 Å and a time unit $\Delta t = 10^{-6}$ s, 1 μm/s translates to $v = 2 \times 10^{-3}$ $l/\Delta t$,[10] which is in an extremely slow range of speeds. Experiments in the companion paper used 0.02−10 μm/s to see the dependence of the nanografted patterns on the AFM tip

(18) Sheehan, P. E.; Whitman, L. J. *Phys. Rev. Lett.* **2002**, *88*, 156104.
(19) Delamarche, E.; Schmid, H.; Bietsch, A.; Larsen, N. B.; Rothuizen, H.; Michel, B.; Biebuyck, H. *J. Phys. Chem. B* **1998**, *102*, 3324.
(20) Jang, J.; Hong, S.; Schatz, G. C.; Ratner, M. A. *J. Chem. Phys.* **2001**, *115*, 2721.
(21) Lavrich, D. J.; Wetterer, S. M.; Bernasek, S. L.; Scoles, G. *J. Phys. Chem. B* **1998**, *102*, 3456.
(22) Ulman, A. *An Introduction to Ultrathin Organic Films, from Langmuir−Blodgett to Self-Assembly*; Academic Press: San Diego, 1991.

speed. It should be noted that, even with the highest speed of 10 μm/s, the tip does not travel one lattice spacing in the unit simulation time Δt. In the simulation, we control the tip speed, v, and the tip width, $(2r_{tip} + 1)$, and delete particles in the area immediately behind the AFM tip. This assumes that the displaced thiol molecules exhibit high enough solubility in normal experimental solution media that they never return to the surface. The standard values are $v = 10^{-3}\ l/\Delta t$ and $r_{tip} = 10l$ (5 nm).

II.c. Nanografting: Enhanced Deposition. For the shaved region of surface, we use the same set of dynamics used for natural-growth self-assembled monolayer formation as described above. This is a reasonable first approximation because the tip speed is extremely small and the role of the tip can be thought of as being limited to shaving. The Reynolds number, *Re*, of a moving micrometer-scale object (AFM tip) with μm/s speed in ethanol is $Re = vL\rho/\eta = (1\ \mu\text{m/s})(1\ \mu\text{m})(0.789\ \text{g/cm}^3)/(1.20 \times 10^{-2}\ \text{g/cm·s}) = 6.6 \times 10^{-7}$, where v and L are the speed and length scale of the moving object and ρ and η are the density and viscosity of the fluid. In a fluid with an *Re* number this small, thermal molecular diffusion is dominant over any inertial motion due to the moving object. Indeed, a moving AFM with μm/s-scale speeds on a bare Au surface does not affect the deposition rate, as demonstrated in a blank experiment in ref 9.

As a second component of our treatment of nanografting, we assume that the deposition probability in a small shaved region immediately behind the tip, an opening bordered by the SAM edges and the relatively big AFM tip, is much higher than in other regions of the Au surface. This assumption arises from the observation that the nanografting time (the total time to obtain a complete monolayer after the start of nanoshaving) is at least an order-of-magnitude shorter than the time for filling the same area by natural-growth deposition. Interestingly, such enhanced deposition is not very sensitive to what we consider factors that control chemical kinetics, such as the thiol concentrations, thiol chain length, thiol chain bulkiness, and even properties of thiol end groups (varying from highly hydrophilic to highly hydrophobic).[9,23] Thus, we propose that the enhanced deposition probability depends only on the spatial confinement, not on chemical details, of the subsystem formed right behind the tip. To define this enhanced deposition probability, the geometry formed by the SAM edge and the tip is described in Figure 1B. The tip surface exposed behind the tip is defined as the tip wall, and the *first* chemisorbed molecule encountered behind the tip is defined as the soft wall. Farther behind the tip and soft wall, the edge of the continuous SAM is defined as the hard wall.

Accordingly, the deposition probability between the tip and soft walls is assumed to be governed by $P' = P + P_s \exp(-\langle h\rangle/\xi)$, where P is the normal deposition probability, P_s ($\gg P$) is the additional geometry-dependent deposition enhancement. In this expression, $\langle h\rangle$ is the average distance from the tip and soft walls, and ξ is the characteristic length of the confined space that leads to deposition enhancement (h in the figure is replaced with the average distance $\langle h\rangle$ to describe two-dimensional nanografting with a finite-width tip). We set $P_s = 0$ in the region between the soft and hard walls because there is no special confined environment in this region, and the deposition probability is simply that of the normal diffusional deposition, P. The physical origin of P_s and the assumed exponential decay factor $\exp(-\langle h\rangle/\xi)$ will be discussed in detail after simulation results are presented in the next section.

Since $P = 10^{-5}$ is determined by the natural-growth SAM, P_s and ξ are new parameters that are needed in nanografting. Their values will be determined by examining experimental data, but standard values that we will consider are: $P_s = 0.01$ ($\gg P = 10^{-5}$) and $\xi = 5l$ (the average length of the thiols C_{10} and C_{18}).

III. Simulation Results and Discussion

III.a. Natural-Growth SAM. We show typical simulation results for natural-growth SAMs in Figure 2A. Assuming that the surface diffusion time scale for alkane thiols on a Au surface is $\Delta t = 10^{-6}$ s, the deposition rates in this simulation are $k = k_{C18} = k_{C10} = 5\ \text{s}^{-1}$. This is related to the concentrations of C_{10} and C_{18} thiols by, $[C_{18}] = k_{C18}/k_{\text{intrinsic,C18}} = 9.88 \times 10^{-4}$ M and $[C_{10}] = k_{C10}/k_{\text{intrinsic,C10}} = 6.15 \times 10^{-3}$ M. The concentration ratio $[C_{10}]/[C_{18}] = 6.22$ leads to a 1:1 surface composition ratio between the two species, because the sticking probabilities or intrinsic adsorption constants for longer-chain thiols are larger, as discussed earlier.

Figure 2A shows large domain structures for the case where the deposition probability $P = (k_{C18}+k_{C10})\Delta t$ is 10^{-5}. If we increase k by a factor of 10, we observe a decrease in domain size, Figure 2C. Physically, this means that we can control the domain size in the SAM by varying the concentrations of thiols in solution, because the higher deposition probability due to the higher concentration means that the physisorbed molecules have less time and room to rearrange themselves.

The size of domains in a particular mixed SAM can be quantified using radial distribution functions, assuming that domain shapes are isotropic. Figure 2B shows the radial distribution functions for Figure 1A. When the $g_{AA}(r)$ ($A = C_{18}$) curve comes down to the mean coverage (i.e., $g(r) = 1$), we can consider that we have reached the C_{18} domain edge. In the same way, when the $g_{AB}(r)$ ($B = C_{10}$) curve comes up to the mean coverage, we can also consider that the same domain edge has been reached. From this point forward, we will define the domain size as the intersection point of these two curves. The domain sizes, (expressed as the radius r_{domain}), for a few choices of the deposition probability are listed in Table 2.

Earlier in the modeling, we introduced many other parameters such as ϵ/k_BT, A_m, f, and θ^c_{loc}. Although the main interest in this work is on the nanografting simulations, it is useful to study the trends in domain size as these parameters are varied. It turns out that larger values of ϵ/k_BT and A_m and smaller values of f, θ^c_{loc} tend to lead to smaller domains. The reason is that, with a constant deposition rate, any factors that hinder surface diffusion, which lets the thiols rearrange themselves to make large domains, will reduce the domain size. Smaller θ^c_{loc} means an earlier phase transition, while smaller f means a broader range of phase transitions for a specified θ^c_{loc}. Larger A_m leads to a shorter physisorption lifetime, and larger ϵ/k_BT means thiol molecules are held back more strongly by same-species nearest neighbors. For example, Figure 2D displays how domain sizes change when the stickiness ϵ/k_BT changes to 1 from 10 (Figure 2A). The third column of Table 2 gives numerical values of the domain radii for this case.

III.b. Nanografted SAM. We consider a $21l$-width ($r = 10l$) flat chisel-like tip horizontally shaving a portion of the 101 ×

(23) Liu, G.-Y. Private communications.

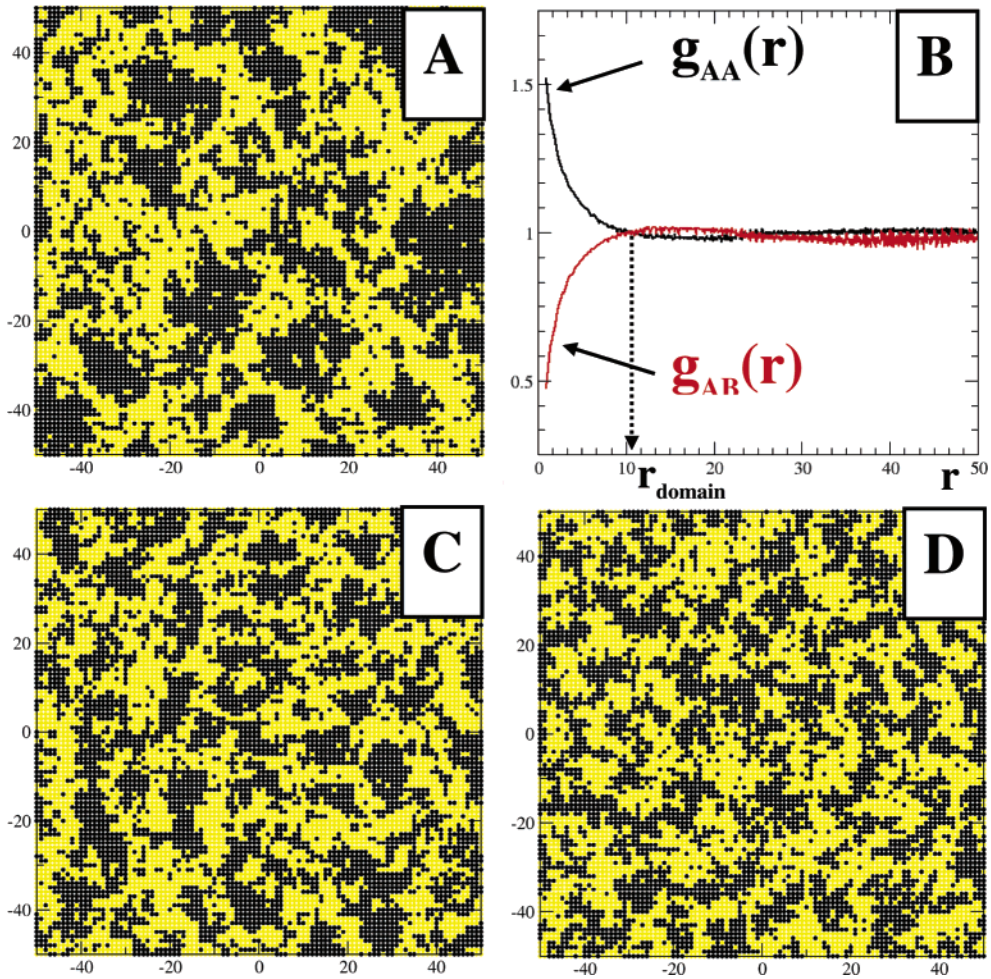

Figure 2. [A] Results for natural growth of a 1:1 binary(C_{18}/C_{10}) mixed SAM. (C_{10} and C_{18} are black and yellow dots, respectively.) $k = k_{C18} = k_{C10}$ is varied to change $P = (k_{C18} + k_{C10})\Delta t$. The other simulation parameters are $\Delta t = 10^{-6}$ s, $\epsilon/k_BT = 1$, $A_m = 10^{11}$ s^{-1}, $f = 20$, $\theta^c_{loc} = 0.9$. [B] Radial distribution function for the monolayer shown in Figure 2A. [C] Natural growth of a 1:1 binary(C_{18}/C_{10}) mixed SAM when the deposition probability, $P = 10^{-4}$, is 10 times higher than in Figure 2A. [D] Natural growth 1:1 binary(C_{18}/C_{10}) mixed SAM when the same-kind particle interaction, $\epsilon/k_BT = 10$, is 10 times higher than in Figure 2A.

Table 2. Domain Radius for Simulation Results Shown in Figure 2

P	$r_{domain}(\epsilon/k_BT = 1)$	$r_{domain}(\epsilon/k_BT = 10)$
10^{-3}	3.2l	2.4l
10^{-4}	5.0l	3.3l
10^{-5}	10.5l	4.8l

101 lattice. These sites belong to $\{(x,y)|\ -45 \le x \le 45,\ -42 \le y \le 41\}$ region of the mixed SAM in Figure 2A, corresponding to the case where the tip center travels from (−45,31) to (45,31), from (45,10) to (−45,10), from (−45,−11) to (45,−11), and from (45,−32) to (−45,−32).

Figure 3 presents results for three different shaving speeds in the range $v = [(10^{-5}-10^{-3})l/\Delta t]$. The results show that different shaving speeds lead to different domain sizes, with the slower tip speed leading to the smaller domain size. The results in Figure 3 (top) are not surprising if we notice that the tip speed $v = 10^{-5}l/\Delta t$ has the same numerical value as the deposition probability P. In fact, the deposition in this case takes place at lattice sites as soon as they are exposed by the tip. We will call this the "critical tip speed", v_c. At speeds larger than the critical tip speed, the domain sizes become larger. This is shown in Figure 3 (middle) and Figure 3 (bottom); however, we note that there is a limiting size that we discuss later.

To have a better overview on the relationship between kinetics and domain size, we plot the total nanografting time (time for completion of both the nanoshaving and self-assembled adsorption) against the tip speed in Figure 4 (top). The dotted straight line represents complete shaving, and the black solid curve indicates the time for getting the SAM back when the role of the tip is limited to shaving only (i.e., there is no enhancement in deposition probability). There is a slope change in the black solid curve near the critical tip speed $v_c = 10^{-5}l/\Delta t$. At speeds lower than v_c, the kinetics is totally governed by tip speed. And there is a switchover between tip-controlled kinetics and deposition-controlled kinetics in the range $[(10^{-5}-10^{-4})l/\Delta t]$. In addition, when the tip speed is equal to or higher than $10^{-3}l/\Delta t$, the tip speed does not really matter as the black solid curve levels off. The domain radius plot, Figure 4 (bottom), shows a gradual change in the domain radius (black solid curve) in the kinetics switchover range (which we denote the "transitional tip-speed range", hereafter) $[(10^{-5}-10^{-3})l/\Delta t]$, for which the domain structures are shown in Figure 3, but basically no change for tip-speeds above $10^{-3}\ l/\Delta t$. The limiting value at the highest tip speed of the domain radius is 7.8l, which is smaller than 10.5l found for the natural growth case. We can attribute this

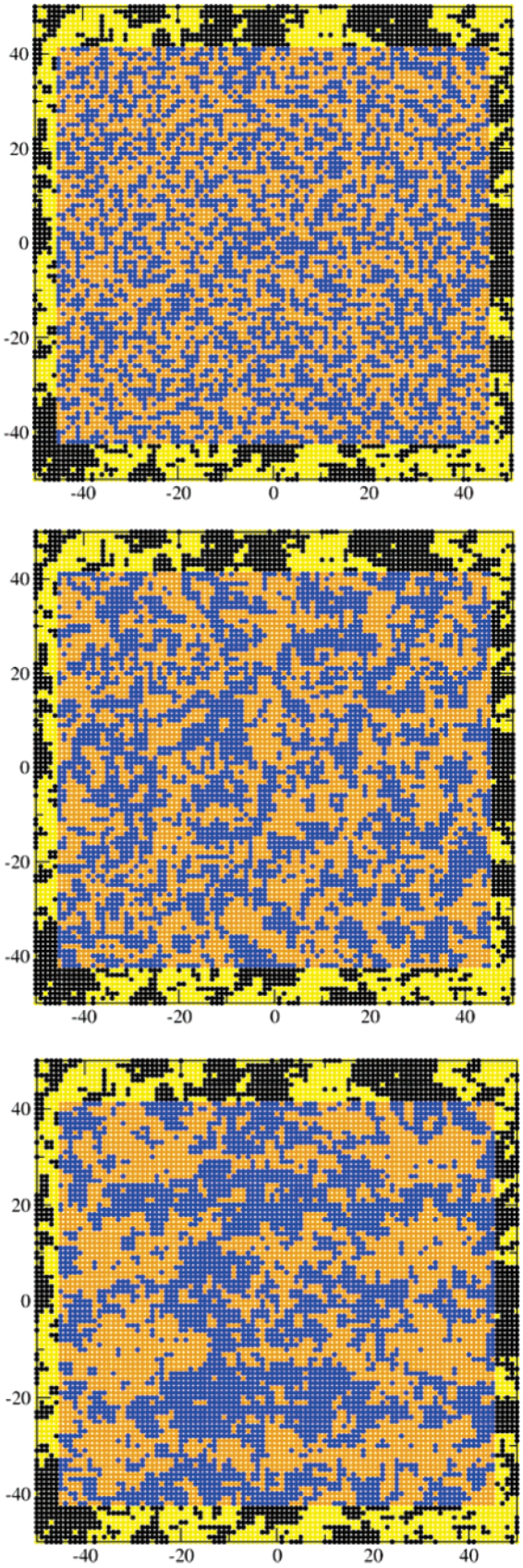

Figure 3. Nanografted SAM structures for three different tip speeds, when the 21l-width tip horizontally shaves the sites belong to $\{(x,y)|\ -45 \le x \le 45,\ -42 \le y \le 41\}$ of the mixed SAM in Figure 2A, with the role of the tip limited to shaving adsorbed molecules only (i.e., no enhanced deposition), for three different tip speeds, $v = 10^{-5}l/\Delta t$, $10^{-4}l/\Delta t$, and $10^{-3}l/\Delta t$. (C_{10} and C_{18} are blue and orange dots in the nanografted area, respectively.)

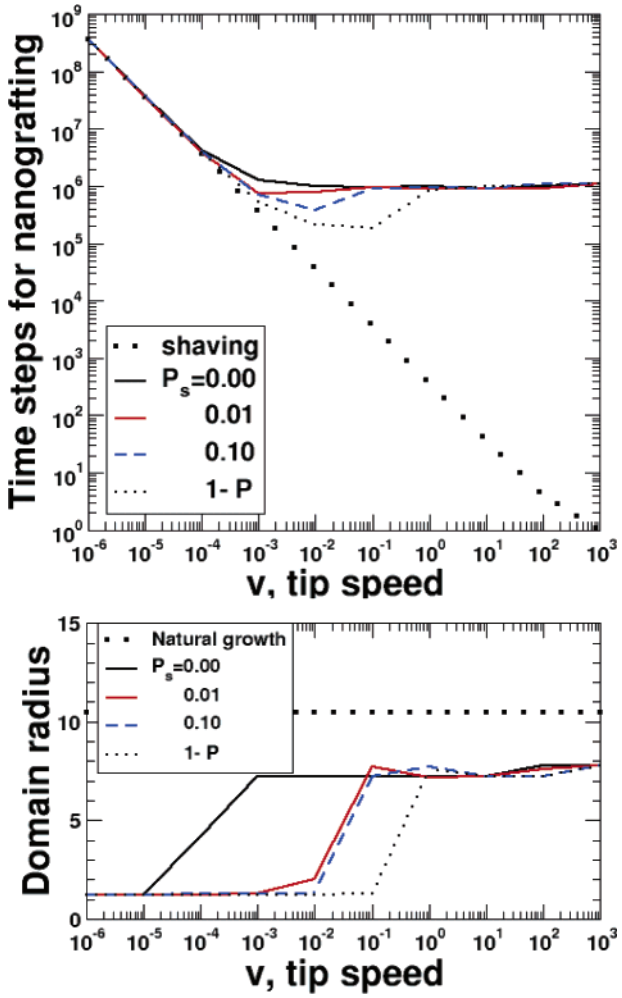

Figure 4. [Top] Total times taken to complete nanografting and [bottom] the domain sizes, when the 21*l*-width tip horizontally shaves the sites belonging to $\{(x,y)|\ -45 \le x \le 45,\ -42 \le y \le 41\}$ of the mixed SAM in Figure 1A. The dotted line represents the time for completing shaving. The other curves represent the times for forming complete monolayers; the black solid line, when the role of the tip is limited to shaving adsorbed molecules; the other curves, when the enhanced deposition right behind the tip is assumed, that is, $P' = P + [P_s \exp(-\langle h \rangle/\xi)]$, where $\xi = 5l$. The thin dotted curve represents the limiting case $P_s = 1 - P$ of maximally enhanced deposition.

domain size reduction to surface diffusion in the *confined* surface area of the shaved region, i.e., the area surrounded by the SAM edges.

To sum up, for the nanografting simulation results when the tip role is limited to shaving only (the black solid curves in Figure 4), we showed that we could regulate the domain size in the shaved region of the mixed SAM by varying the tip speed. This trend agrees well with experimental observations.[10] Although this local control over domain size is one of the major advantages of the nanografting technology over traditional solution-based methods,[10] the black solid curve in Figure 4 (top) also tells us something that is in disagreement with what is observed in the nanografting experiments.[9,10] While it was experimentally found that nanografting is at least an order-of-magnitude faster than natural-growth self-assembly, our simulation shows even slower kinetics (larger number of time steps) in the transitional tip-speed range.

The remaining simulation and discussion will be devoted to studying the missing fast kinetics that arises if we use the

natural-growth model without any modifications. Obviously, the very fast SAM formation in nanografting should be ascribed to some sort of fast deposition of alkane thiols onto the Au surface, but it is not certain what microscopic properties of the system make deposition enhanced. Our phenomenological simulation does not have the capability to reveal the origin of enhanced deposition, but at least it provides a molecular-level description of self-assembly during actual nanografting, i.e. molecules may follow natural growth or SCSA, depending on the transient spatial confinement. This exercise narrows down the possibilities, as we now show using the $P_s > 0$ results in Figure 4.

In the previous section, we defined the tip wall, the soft SAM wall, the hard SAM wall, and the enhancement in deposition probability at sites between the tip wall and the soft wall. This probability is given by $P' = P + [P_s \exp(-\langle h \rangle/\xi)]$, where $\langle h \rangle$ is the average distance between the tip and soft walls, and the P_s ($\gg P$) and ξ are two new parameters that are needed for nanografting. In Figure 4, the other three curves (red solid, blue dashed, black thin dotted) are simulation results for $P_s = 0.01$, 0.10, 1.00, respectively. Here, the characteristic length scale ξ in the enhanced deposition is taken to be the average thiol chain length, $\xi = 5l$. Note that there are "dips" in the nanografting time plot, Figure 4 (top). As we increase the enhanced deposition parameter P_s, the dip becomes deeper, meaning that the speed of nanografting is increased. Choosing $P_s = 1.0$ increases this speed by up to a factor of 10. At the same time, when we look at Figure 4 (bottom), it is clear that we can still control the domain size, but the transitional tip-speed range is shifted to higher-tip speeds. This behavior closely matches what is observed in the nanografting experiments.

Figure 5 shows the nanografted regions, with a constant $P_s = 0.01$, shaved at tip speeds that cover the transitional range in Figure 4. Again, we can control the domain size as in Figure 3, but now the whole nanografting process is much faster.

To investigate further the effect of tip speed on the nanografted patterns of Figure 5, we show in Figure 6 snapshots when the tip shaves only one-eighth of the total nanografting area of Figure 5. (The tip position at the end of the shave is at $(x,y) = (0,31)$.) In the lower speed ($v = 0.001l/\Delta t$) result, adsorption is quickly followed by chemisorption due to high local coverage (physically, the high lateral pressure). At the opposite extreme ($v = 0.100l/\Delta t$), only a tiny fraction of the open sites are occupied, and basically all of the particles are deposited in the shaved region are eligible for surface diffusion. At intermediate speed ($v = 0.01l/\Delta t$), the tip leaves behind an incomplete monolayer. While some of adsorbed molecules are in their chemisorbed state, other molecules keep diffusing to give as large domains as they can make.

Figure 7 presents snapshots of the deposition, here with the tip speed fixed at $v = 0.01l/\Delta t$ and with different choices of the enhanced deposition probability. This shows that only a small fraction of open sites are filled with physisorbed molecules when there is no enhanced deposition ($P_s = 0.00$). For $P_s = 0.01$, there is quick but incomplete monolayer formation, and for $P_s = 0.10$ there is quick complete monolayer formation (almost simultaneous deposition and transition into the chemisorbed state). A more detailed analysis of Figure 7 is presented in Figure 8, where we show the three wall positions as the tip travels from $(-45,31)$ to $(45,31)$. Here we see that, when $P_s = 0$, the two kinds of SAM walls do not move at all. However as the deposition probability is increased, the soft and hard SAM walls quickly follow the tip wall. We varied the tip width ($2r_{tip}$

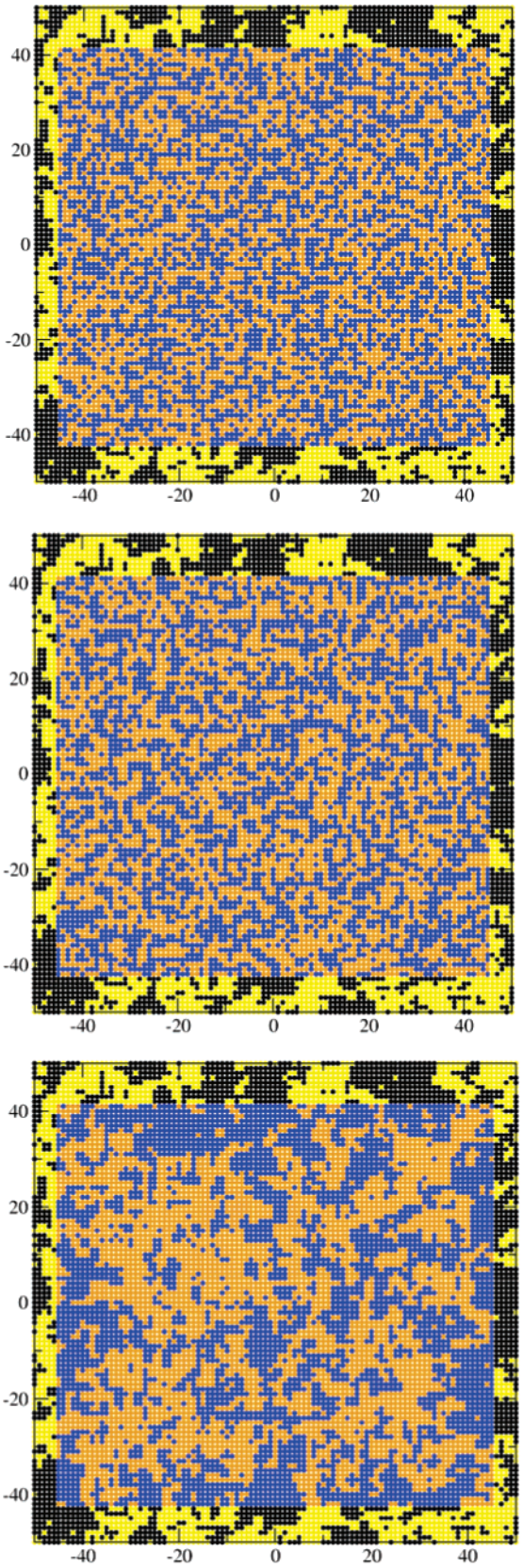

Figure 5. Nanografted SAM when the enhanced deposition probability, $P_s = 0.01$, is employed, for tip speeds, $v = 10^{-3}l/\Delta t$, $10^{-2}l/\Delta t$, and $10^{-1}l/\Delta t$. (C_{10} and C_{18} are blue and orange dots, respectively, in the nanografted area.)

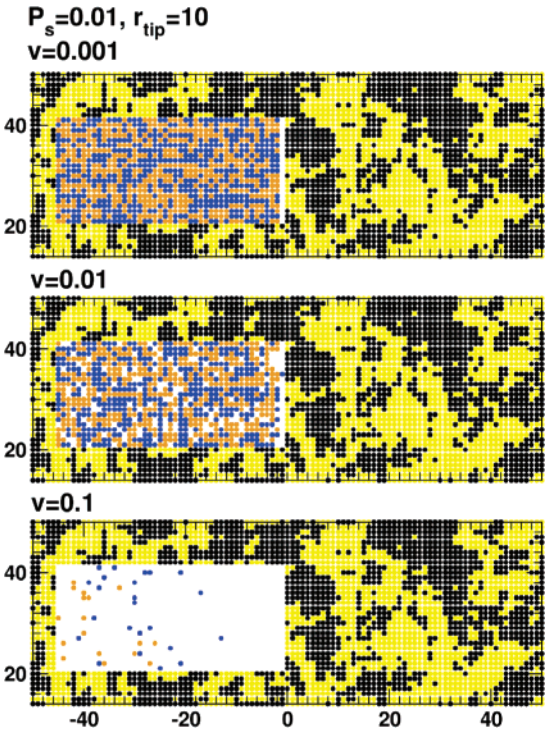

Figure 6. Snapshots of nanografting, for a constant enhanced deposition $P_s = 0.01$, when the first one-eighth of the area has been shaved at the tip speeds, $\upsilon = 10^{-3}l/\Delta t$, $10^{-2}l/\Delta t$, and $10^{-1}l/\Delta t$.

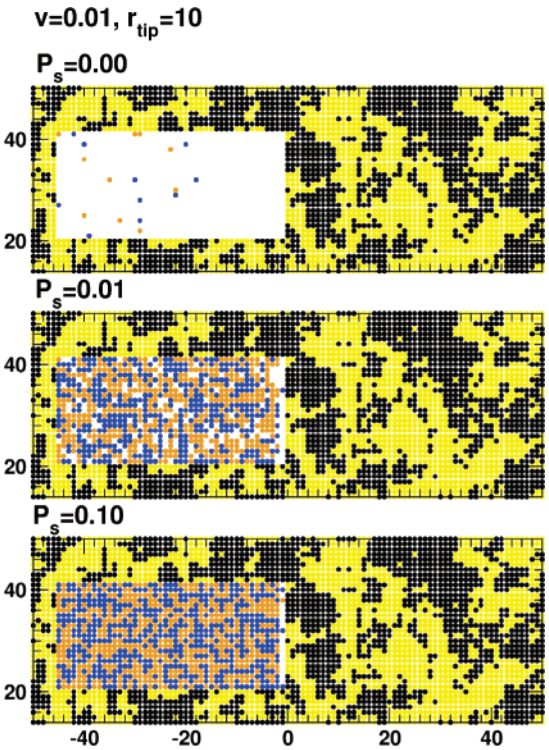

Figure 7. Snapshots of nanografting, for the same tip speed $\upsilon = 10^{-2}l/\Delta t$, when the first one-eighth of the area has been shaved as the enhanced deposition probability P_s is turned on, from 0.00 to 0.01, and from 0.01 to 0.10. The tip position in both figures is (0,31).

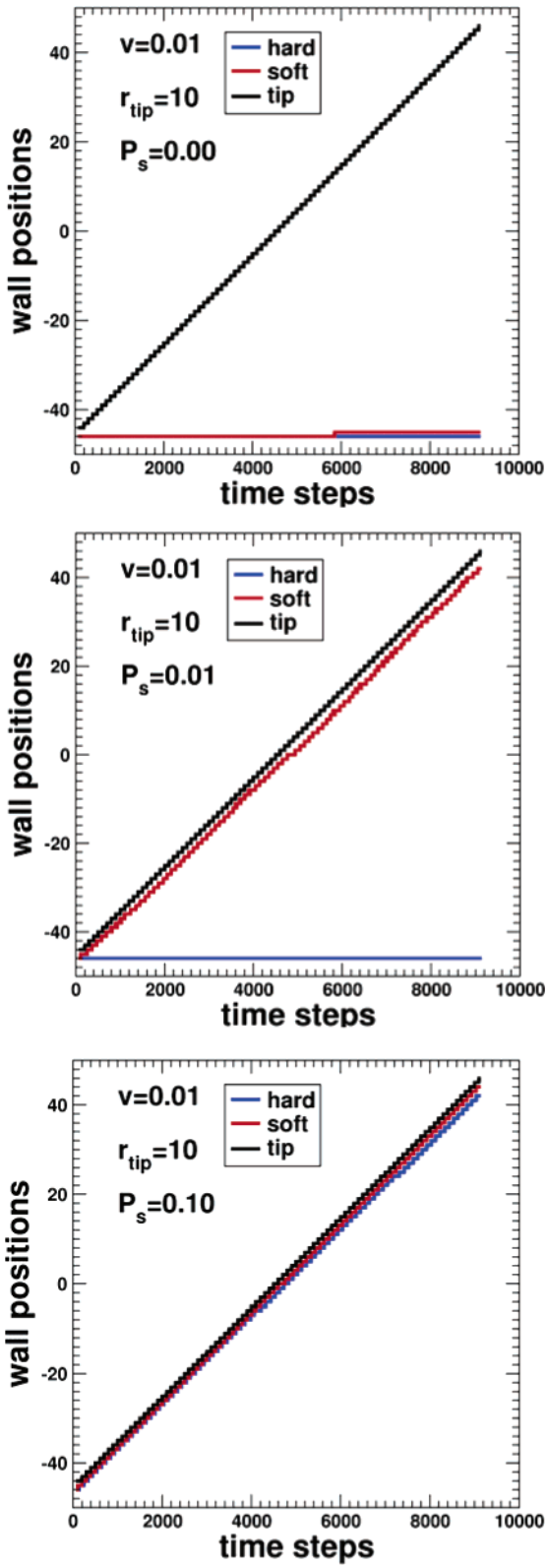

Figure 8. Tip, soft, and hard wall positions as the nanografting progresses under the conditions of Figure 7. The tip travels from $x = -45$ to 45 at $\upsilon = 10^{-2}$. The nanografted SAM structures with a few different tip speeds, when the 21l-width tip horizontally shaves the sites belong to $\{(x,y)|-45 \le x \le 45, -42 \le y \le 41\}$ of the mixed SAM in Figure 2A, when the role of tip is limited to shaving adsorbed molecules only, with the three tip speeds, $\upsilon = 10^{-5}l/\Delta t$, $10^{-4}l/\Delta t$, and $10^{-3}l/\Delta t$. (C_{10} and C_{18} are blue and orange dots, respectively, in the nanografted area.)

+ 1) from $r_{tip} = 0$ to 20, and checked the wall positions, and we found that the results (not shown in this work) exhibit the same trends, regardless of tip width.

We can summarize our simulation results for nanografting with enhanced deposition as follows. Given the single assumption that there exists enhancement of deposition in a small, confined region immediately behind the tip, we can reproduce

the experimental deposition results fairly well. In particular, we find up to one-order-of-magnitude faster kinetics in nanografting and that the faster the AFM tip displaces adsorbed particles from a perfect monolayer, the more space and time that is available for the deposited thiol molecules to rearrange themselves to form larger domains.

In an earlier experimental mechanistic study,[9] Liu and coworkers suggested a different reaction pathway for the nanografted thiol molecules. They proposed a spatially constrained self-assembly (SCSA) mechanism to account for the faster kinetics of the nanografting experiment. In SCSA, those thiol molecules that have standing-up configurations are preferentially adsorbed in spatially confined environments due to less steric hindrance compared to those having the other configurations. This lowers the activation energy for adsorption, leading to accelerated kinetics.

This SCSA mechanism can be understood in terms of our model using the following argument. In general, the deposition rate, k, is given as the product of the sticking probability, S, and the flux, J, toward the surface. In the SCSA mechanism, the basic assumption is that, while the flux into a small, confined region is the same molecular diffusional flux as in NSA, i.e., $J \approx C\upsilon_T$, the sticking probability is greatly enhanced due to a lowered activation energy. For instance, when a thiol molecule adsorbs on a bare Au surface in a lying-down configuration, the sticking coefficient can be empirically modeled using $S_0 \approx [S_{0m} \exp(-E_d/RT)]$, where $S_{0m} \approx 1$ and $E_d = 45$ kJ/mol $-$ (0.65 kJ/mol)N_{CH_2},[16] as we discussed earlier. This expression for E_d reflects the fact that longer-chain thiol molecules tend to be stickier toward the Au surface. In fact, we used this constant sticking coefficient concept to calculate the deposition probabilities in simulating natural growth.

In the SCSA mechanism for nanografting, however, thiol molecules enter the small, confined space in standing-up configurations, and the aforementioned empirical model should be modified. It is likely that the frequency factor S_{0m} decreases slightly to S_{sm} ($< S_{0m}$) because only portions of all possible configurations are accepted. However, the precise value of S_{sm} is not important in this analysis. More important is the fact that when a thiol molecule enters a small, confined, shaved region in a standing-up configuration, the activation energy E_s for reaction of this molecule with the surface is expected to be smaller than the activation energy E_d for reaction of a lying-down molecule with the surface, i.e., $E_s < E_d$. If we assume that E_s approaches E_d linearly as the shaved space widens, we may write the activation energy in the form $E_s + \Delta E\langle h\rangle/\zeta$ (for values less than E_d), where ΔE is the activation energy increment for some distance increment ζ. Then, the new sticking coefficient in the spatially confined environment becomes $[S_{sm} \exp(-E_s/RT) \exp(-\langle h\rangle/\xi)]$, with the rescaled distance increment $\xi = \zeta(RT/\Delta E)$. Setting $S_s = [S_{sm} \exp(-E_s/RT)]$, the sticking coefficient will be of the form, $[S_s \exp(-\langle h\rangle/\xi)]$, which makes the deposition probability be $[P_s \exp(-\langle h\rangle/\xi)]$, thus matching our model.

Another explanation for the enhanced deposition in nanografting involves the assumption that it is the molecular flux rather than the sticking probability that is enhanced compared to natural deposition. This argument follows because nanografting requires that molecules flow or diffuse to the shaved opening in the SAM, and there are a number of factors that can make this process different compared to diffusion to the surface in natural deposition. This opening has dimensions which depend on tip speed but would be on the order of <1 nm times the tip width for slow tips. The wall-like structure around the opening provides a vertical dimension as well. As a result, it is worth considering if transport of molecules to the surface can be characterized as thermal molecular diffusion, and if it is diffusion, what is the effective dimensionality of it, and does the tip serve to control the flow.

In normal natural growth, we assumed that the sticking probability S_0 is constant with time and that there is a constant thiol flux toward the surface $J \approx C\upsilon_T$. The constant flux assumption is based on the idea that the diffusion layer where the concentration gradient is formed is sufficiently thin and does not grow much with time. As a matter of fact, this is an application of the planar diffusion model, in which molecules are transported along the concentration gradient in a thin layer toward an infinite flat surface. The diffusion layer thickness, δ, depends on the diffusion constant D_m of thiols in solution and the adsorption rate at the surface. In general the thickness varies with time, but a very rough estimate can be made via the Nernst layer approximation $J \approx D_m(C - C_0)/\delta$, where C_0 is the concentration right next to the surface.[24] Assuming that $J \approx C\upsilon_T$ and $C_0 \approx 0$, we obtain $\delta \approx D_m/\upsilon_T \approx (10^{-6}$ cm^2/s)/(10^3 cm/s) $=$ (0.01 nm) at room temperature.[25] The small value obtained suggests that the molecules have a solution-like density distribution until just above the surface.

In nanografting, particularly at slower tip speeds, however, a model similar to spherical diffusion would be more appropriate, in which the molecular flux is maintained radially constant and mass transfer is directed toward a small area or region, such as that which occurs with ultramicroelectrodes.[26] The molecular flux toward a disk-shaped ultramicroelectrode is given by $J \approx CD_m(1/\delta + 1/r_a)$ where r_a is the radius of the disk.[27] The assumption of a fixed sticking coefficient accordingly leads to the deposition probability model $P(1 + \delta/r_a)$, which may be used in the simulations. For a simulation, we may consider that the diffusion layer thickness, δ, is a new parameter, and set $r_a = \langle h\rangle$ at each simulation step. At the beginning of nanografting, we can assume $\langle h\rangle \approx \upsilon\Delta t$, and then the condition for which deposition is enhanced due to spherical diffusion is determined by the condition $\upsilon \ll \delta/\Delta t$ where v is the tip speed. For the δ value estimated above and $\Delta t = 10^{-6}$ s (the value used in our simulation), this leads to $\upsilon \ll 0.02l/\Delta t = 10\ \mu$m/s. The variation of the deposition results with tip speed (subject to this inequality) in a mixed SAM nanografting simulation will lead to changes in the lateral heterogeneity that provide a direct measure of the relative importance of the two diffusion models.

Most likely both of these two factors, sticking probability and flux enhancement, play some role in the nanografting process. Although our model has represented the enhanced deposition in terms of sticking, flux enhancement would lead to the same or similar algorithm, so that it is not possible to distinguish these factors here. Thus, more theory (closer to the

(24) Levich, V. G. *Physicochemical Hydrodynamics*; Prentice-Hall: Englewood Cliffs, 1962.
(25) See ref 16 for D_m values for thiols in solution media.
(26) Bard, A. J.; Abruña, H. D.; Chidsey, C. E.; Faulkner, L. R.; Feldberg, S. W.; Itaya, K.; Majda, M.; Melroy, O.; Murray, R. W.; Porter, M. D.; Soriaga, M. P.; White, H. S. *J. Phys. Chem.* **1993**, *97*, 7147.
(27) Štulík, K.; Amatore, C.; Holub, K.; Mareèek, V.; Kutner, W. *Pure Appl. Chem.* **2000**, *72*, 1483.

atomic scale) and more experiments are needed to cleanly separate these effects.

Another aspect of SAM growth needs to be mentioned briefly. The self-assembly of molecules into natural-growth SAMs is subject to exchange of molecules between the surface and solution phases, and normally the longer-chain molecules have more favorable free energies, leading to preferential C_{18} deposition, C_{18} (sol) + C_{10} −Au (s) → C_{10} (sol) + C_{18} −Au (s). However, the companion paper[10] shows that this equilibrating process is so slow that nearly the same SAM structures are maintained for as long as a few months. Therefore, our kinetic model, which neglects this exchange, can be considered to capture most of the molecular self-assembly process, leading to the final SAM and domain structures seen in the experiments.

IV. Concluding Remarks

We developed a simple phenomenological Kinetic Monte Carlo model of natural and nanografted deposition for alkane thiols on gold surfaces that successfully describes many experimental results, especially the difference in raft domain structures that arises when deposition is performed with a mixture of two different alkane thiols. The model includes deposition, surface diffusion, and molecular phase-transition processes, with interactions between alkane thiols leading to different diffusion behavior of alkanes in a binary mixture, depending on what molecules surround the diffusing molecule. With this model, we have confirmed that the size of the domain structures found in naturally grown monolayers can be controlled by the binary thiol solution concentrations. For nanografting, we introduced the key assumption that the deposition probability is higher in the region of the surface confined between the AFM tip and the SAM edges. Our simulations showed that this assumption leads to fast kinetics in the nanografting procedure as well as the capability of the AFM tip to regulate domain size in the deposition of binary mixtures in nanometer-scale local areas. In particular, homogeneous film formation occurs for slow tip speeds, but domain formation dominates for fast tip speeds, similar to what is found in the experiments. To our knowledge, our work is the first attempt to model and simulate nanografting, and thus, the results are expected to serve as a starting point for further theoretical and simulation research.

The key assumption of deposition enhancement immediately behind the tip can be attributed to enhanced sticking probability or enhanced molecular flux in the spatially confined environment behind the AFM tip. The possible physical origins of the enhancement were discussed, but the level of detail in our model is not sufficient to sort out sticking versus flux enhancement. Further studies of these issues using molecular dynamics simulations and quantum mechanics calculations are needed to sort out these issues.

Acknowledgment. This research was supported by the National Science Foundation (Grant CHE-0550497). We have greatly benefited from extensive discussions and preliminary data from Gang-Yu Liu.

Supporting Information Available: Four more figures are provided which show simulation results when parameter values are changed from those used to generate Figure 4. This material is available free of charge via the Internet at http://pubs.acs.org.

JA063138B